Pressure Effect in a Shock-Wave–Plasma Interaction Induced by a Focused Laser Pulse

A. Sasoh,[1] T. Ohtani,[2,*] and K. Mori[1]

[1]*Department of Aerospace Engineering, Nagoya University, Nagoya 464-8603, Japan*
[2]*Department of Aerospace Engineering, Tohoku University, Sendai 980-8579, Japan*

(Received 5 July 2006; published 16 November 2006)

The effect of ambient pressure on the interaction between a laser plasma bubble and a shock wave involving a Richtmyer-Meshkov instability was experimentally studied via framing Schlieren visualization. A sharp plasma interface could be formed without any separation material that causes undesired disturbances. The fundamental vortex structure which was produced via baroclinic effects was self-similar with respect to the laser energy-ambient pressure ratio. Yet, the higher the ambient pressure, the more high-wave-number instabilities were enhanced so as to contaminate the self-similarity.

DOI: 10.1103/PhysRevLett.97.205004 PACS numbers: 52.57.Fg, 52.30.−q, 52.38.−r

The fluid-dynamic instability appearing in impulsively loaded flows, which is referred to as Richtmyer-Meshkov instability [1,2], is a research topic of considerable importance in astrophysics and fusion research, for instance. This type of instability is initiated by baroclinic vorticity production that is in proportion to the vector product of the density and pressure gradients; the interface instability grows irrespective of the sign of the product, while the direction of the growth depends on it. The theoretical model of instability initiation was developed by Richtmyer [1]. However, the long-term flow evolution induced by this instability is so complicated that few details can be quantitatively predicted even by numerical simulation, thus warranting further experimental studies. Most published work related to this instability has used the Atwood number and shock Mach number as primary control parameters. To the authors' knowledge, few studies have been performed concerning the effect of the ambient pressure as an independent parameter, and, in particular, whether or not the flow becomes self-similar irrespective of the ambient pressure if these control parameters are unchanged. Hereafter, this effect will be referred to as the ''pressure effect.'' Experimental studies of this effect using existing methodologies are hampered by technical problems such as the membrane disturbance [3,4].

Many studies on Richtmyer-Meshkov instability have been conducted using shock tubes. When a sliding sheet is used to separate prefilled test gases, the interface becomes diffusive while it is being opened mechanically [5,6]; the thickness of the diffusive zone depends on the ambient pressure. The pioneering work of Meshkov [2] and many following works employ a plastic membrane [7–12]. Erez *et al.* [13] concluded that the presence of a membrane is important to the initial stage of a small amplitude. Even using a soap film to form the membrane, its impact is not completely eliminated [14–16]. In Ref. [15], small-scale perturbations appearing on the interface are attributed to the nonuniformity of the soap membrane. However, as will be shown later, this speculation is questionable.

A membraneless method to make an interface has been employed by supplying a gas flow as a sheet or column(s) [17–19]. Jones *et al.* [20,21] developed a technique to form an interface in a vertical shock tube as the boundary of opposing gas flows, both of which exit the shock tube to the ambient atmosphere. Although the interface has a diffusive zone, it becomes thinner after experiencing the shock compression, and an evolution of the sharp interface can be observed. Yet, in this case the test section pressure is impractically difficult to vary with an incident shock Mach number being kept constant, because usually the test pressure should be maintained at a level only slightly higher than the atmospheric value. The effects of the wall boundary layer is another serious problem in applying shock tube technology to the present problem [22–24].

Sankin *et al.* [25] studied the interactions between a laser-generated bubble and a shock wave in water. Although a laser-induced bubble can be generated relatively easily in water, in gaseous media the breakdown threshold is sensitive to the local laser power density; with optics of a long focal length a spherical bubble is difficult to produce. Without any special modification, short focal length optics may itself disturb the flow of the interest.

In this study, the pressure effect on a laser plasma-shock-wave interaction that involves Richtmyer-Meshkov instability is studied with a new experimental arrangement, in which a sharp interface is generated without undesired membrane-oriented disturbances, and the reflected shock wave driven by the plasma itself is used for the interaction. Figure 1 schematically illustrates the test section of the present experiment. The cylindrical test chamber was 300 mm in inner diameter and 300 mm in length along the horizontal axis. Near the center of the chamber, an aluminum parabolic mirror was set so that its axis was aligned with a radius of the test chamber. The diameter of the parabola was 42 mm, the focal length 21 mm. A TEA (transversely excited atmospheric) CO_2 laser pulse (wavelength; 10.6 μm) was directed along the parabola axis through a ZnSe window. The output laser beam had a diameter of 50 mm. The effective beam diameter incident

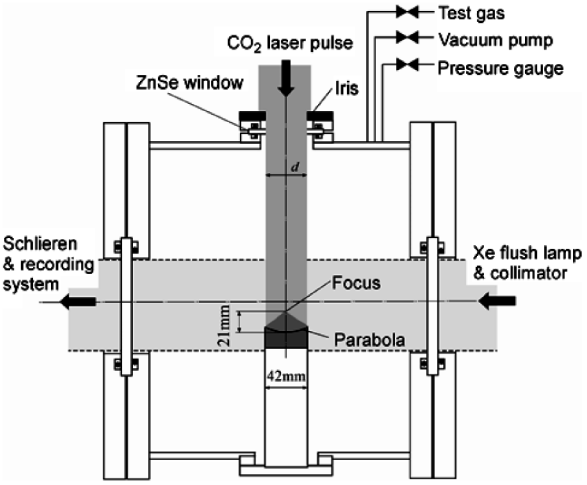

FIG. 1. Schematic diagram of test chamber.

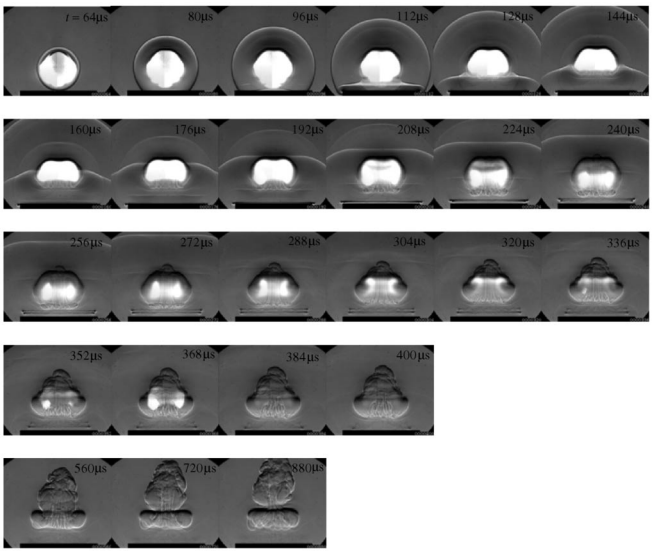

FIG. 2. Framing Schlieren images, Kr, $P_0 = 40$ kPa, $E = 3.61$ J, $d = 36$ mm, $\Delta t = 16\ \mu$s (up to $t = 400\ \mu$s)/160 μs ($t > 400\ \mu$s).

onto the parabola was controlled by the diameter of the iris placed above the window. The full width at half maximum of the primary laser power peak was 0.2 μs; 90% of the total energy E was irradiated in 3 μs. The peak power density effectively incident upon the parabola was 7×10^9 W/m^2 for a total laser energy of 10 J. The effective laser pulse energy was measured with an energy meter (GENTEC ED-500-LIR) placed above the parabola in the test chamber when it was open to the atmosphere.

Initially, the test chamber was evacuated using a turbomolecular pump that was backed by a rotary pump to 10^{-3} Pa. Then the test gas was introduced to the ''ambient'' pressure P_0. In our previous work [26], it was confirmed that flow physics were unchanged among argon, krypton, and xenon. Therefore, in this study, only one species, krypton, was examined as their representative.

Time evolution of the laser-induced flow was visualized through a Schlieren system, recorded onto a high-speed framing camera (HyperVision HPV-1, Shimazu Co., resolution 312×260 pixels). In this camera, one hundred images were sequentially recorded onto a single CCD device, so that the sensitivity distribution in each frame was fully reproducible. A xenon flush lamp was used as the light source. The collimated light beam for the visualization was supplied along the axis of the test chamber.

Figure 2 shows an example of the visualized laser-induced events over the parabola [27]. It should be noted that in all the figures shown hereafter the contrast and brightness are not software processed; they all are rough pictures. Time elapsed after the laser pulse initiation is designated by t; even in the first frame at $t = 64\ \mu$s the laser pulse has already terminated. During the laser pulse, the central radiating region was directly heated through inverse bremsstrahlung. This region hereafter will be referred to as a ''plasma bubble.'' At $t = 64\ \mu$s–96 μs, it was shaped almost as a sphere, but being influenced by laser power absorption processes its bottom part slightly extruded downward. This ''jetting'' has been observed in other works [28–30] and has been explained as relating to unsteady pressure variation around the focus. However, under the present experimental conditions, this jetting motion was beaten by the proceeding baroclinic motion, which will be discussed later.

During the expansion of the plasma bubble, a spherical shock wave was driven forward. The incident spherical shock wave was reflected on the surface of the parabola, as was observed at $t = 96\ \mu$s and thereafter. When a spherical acoustic wave that originates in the focus is reflected on a parabola, a plane wave is reflected. The observed reflected shock wave was primarily planar and interacted with the almost-spherical plasma bubble, thereby forming a baroclinic interaction, while the geometrical simplicity was degraded to some extent by several nonideal mechanisms, that is, the reflected wave was a shock wave which had nonlinear characteristics; the incident spherical shock wave was not perfectly centered at the focus; the plasma jetting deformed the plasma shape; and the incident shock wave diffracted around the edge of the parabola so that the reflected shock wave was attenuated from the periphery to the center. Since the speed of sound is higher in the plasma bubble than in the surrounding gas, the reflected shock wave traveled through the plasma faster than through the surrounding gas [15]. As a result, the bottom interface became distorted before the arrival of the reflected shock wave in the surrounding gas.

The baroclinic vorticity production rate is given by

$$\left.\frac{\partial \boldsymbol{\omega}}{\partial t}\right|_b = \frac{1}{\rho^2} \nabla\rho \times \nabla P \qquad (1)$$

where P, ρ, and $\boldsymbol{\omega}$ designate pressure, density, and vorticity, respectively. Cartesian coordinates are assumed in order to simplify the explanations (although the fundamental configuration is actually axisymmetric), with x in the horizontal direction, y vertical (coincident to the axis of symmetry), and z normal to the paper. Across the plasma

bubble, $\nabla\rho$ has an effective negative x component in the left half, and positive in the right half. The reflected shock wave yields an effective negative pressure gradient in the y direction. As a result, a positive-z vorticity is produced in the left, negative in the right, so that the curvature of the plasma bubble at the bottom becomes inverted. This process was observed from $t = 128$ μs to 192 μs. In particular, from $t = 144$ μs onwards, the interface, which is recognized as the discontinuity of radiation emission intensity, became concave. Being penetrated by the ambient gas flow from the bottom, the plasma bubble assumed the shape of a jellyfish [15]. From $t = 224$ μs to 336 μs the radiation emission from the plasma bubble acted as a good particle tracer; its vortex motion could be clearly observed, and the plasma bubble formed a toroidal shape [31,32]. The ''bubble reversal'' [15] started at $t = 240$ μs; a hump at the top of the plasma bubble appeared and was extruded upward. The ambient gas flowed through the plasma torus and was ejected upwards. The head of the hump was strongly perturbed due to the interaction between the ambient gas flow and the plasma bubble. As was reported in Ref. [15], the plasma formed as double vortex rings, with the upper portion developing from that which was originally the lower part, and the lower one from the upper part.

Based on the inviscid compressible flow relations, the flow evolution is self-similar with respect to E_b/P_0, where E_b denotes the effective blast wave energy. The shock Mach number M_s measured at a point becomes a function of E_b/P_0. In reality, some energy is lost from the laser energy, not contributing to the blast wave motion. Here, the effective energy conversion efficiency η is defined by

$$\eta = \frac{E_b}{E}, \tag{2}$$

where E denotes the incident laser pulse energy. With the value of η given, M_s becomes a function of E/P_0 [33–35] with the quasi-self-similar solution of Ref. [36] being used as the reference. Figure 3 shows the variation of M_s, measured at a radius of 25 mm from the center axis of the parabola, plotted as a function of E/P_0. Those experimental data fit to an $\eta \approx 0.2$ curve with ± 0.1 scatter. Although the scatter is not necessarily trivial, a clear dependence of η on P_0 or d is not obtained; the large-scale flow evolution is primarily depends on E/P_0.

Figure 4 shows Schlieren images observed under four operation conditions at almost constant E/P_0. Within the jitter of the time origin, the images are synchronized with each other. As shown in Fig. 3, the large-scale flow evolution, including the bubble reversal, was similar with respect to time. However, the higher the ambient pressure, the more small-scale perturbations were enhanced; for example, the central bubble at $t = 1008$ μs is an almost ellipsoid for $P_0 = 10$ kPa, whereas it is subject to perturbations on half-diameter scales for $P_0 = 20$ kPa, up to about one-tenth scales for $P_0 = 40$ kPa and much finer scales for $P_0 = 100$ kPa. In Ref. [15], at the atmospheric pressure, such small-scale perturbations are also reported;

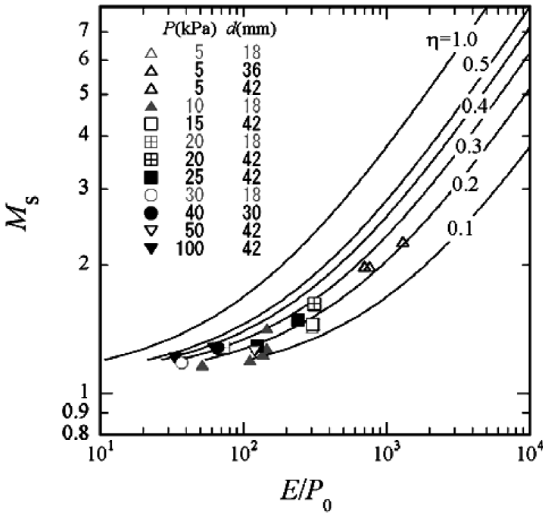

FIG. 3. M_s at $r = 25$ mm vs E/P_0. The error in M_s, which is caused mainly by framing interval duration, is $\pm 5\%$. That in E/P_0, which is caused mainly by shot-to-shot scatter in E, is $\pm 2\%$.

the authors attributed them to the nonuniformity of the soap bubble. Since they are reproduced in the present experiments in which no separation material was used, those perturbations should be caused by fluid dynamics.

It is necessary to examine the effect of the sensitivity of the Schlieren visualization. Because the contrast of the Schlieren image originates in the diffraction of reference beams, which is proportional to the density level, the higher the ambient pressure the more enhanced the contrast becomes. However, looking at the images at $t = 1008$ μs,

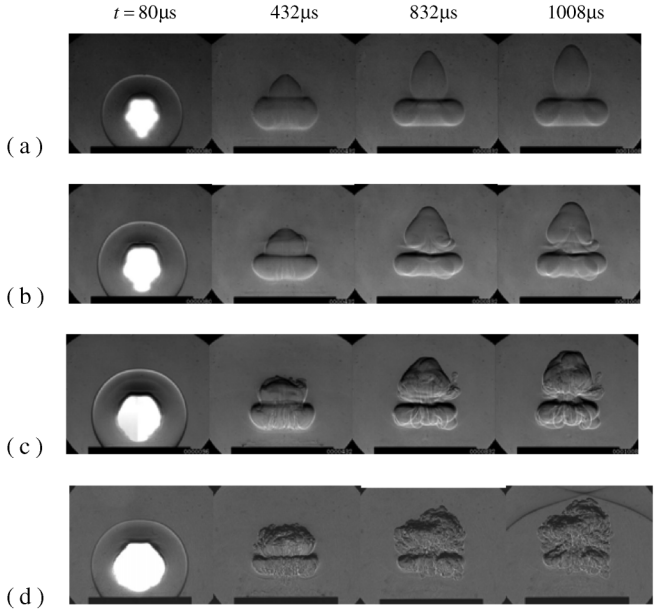

FIG. 4. Framing Schlieren images, Kr, $E/P_0 = 6.7 \pm 0.5 \times 10^{-5}$ J/Pa, (a) $P_0 = 10$ kPa, $E = 0.69$ J, $d = 18$ mm, (b) 20 kPa, 1.44 J, 18 mm, (c) 40 kPa, 2.69 J, 30 mm, (d) 100 kPa, 6.20 J, 42 mm.

the large-scale structure of the plasma bubbles differs greatly. Therefore, the difference in the earlier bubble shape is physical, not due to contrast enhancement in the visualization. In these experiments, in order to tune the laser energy, the iris diameter d was also adjusted. As seen in Fig. 3, its effect on the large-scale flow patterns is not critical. Moreover, as is discussed in Ref. [34], the small-scale perturbations were not explicitly related to d.

At present, the cause for this pressure effect is not fully understood. A possible mechanism is Rayleigh-Taylor instability [37,38]: In general, an interface has inherent perturbations. The higher P_0, the larger the dominant wave number of perturbation k becomes. Since in Rayleigh-Taylor instability, the growth rate of the perturbation scales with $\exp(t\sqrt{gkA})$, where g and A designate the apparent acceleration measured on the interface and Atwood number, respectively. The rate is increased with increasing k and hence P_0. In an overexpansion phase in the plasma bubble bounce motion, the interface experiences deceleration. Because the density in the plasma bubble is lower than that in the surroundings these interface instabilities grow over time. Through the interaction with the reflected shock wave, these instabilities should be enhanced. The validation of this idea warrants further investigations.

The present experiments study the interactions between the laser-generated plasma bubble and the shock wave, which are induced by the same laser pulse irradiation and lead to Richtmyer-Meshkov instability. A sharp interface over a single test gas species is produced without any material and disturbance associated with the separation, and the effect of the ambient pressure on the flow evolution can be systematically investigated. Although the large-scale baroclinic vortex motion is similar with respect to E/P_0, small-scale perturbations are enhanced at high ambient pressures thereby violating the self-similarity. In later times the baroclinically driven flow motion will induce Kelvin-Helmholtz instability and turbulent mixing, on which the initial-stage perturbations dealt in this paper are expected to impose significant impacts, thereby warranting further investigations.

This work was supported by Grant-in-Aid for Scientific Research, Category S, No. 13852014 funded by Japan Society for the Promotion of Science, and by Priority Area No. 422 ''Dynamics of Volcanic Explosion'' funded by Ministry of Education, Culture, Sports, Science and Technology, Japan. The experiments were conducted at the Institute of Fluid Science, Tohoku University, Sendai, Japan, where all of the authors worked. The authors appreciate valuable technical support from Mr. Toshihiro Ogawa, Mr. Kazuo Asano, Mr. Makoto Kato, Mr. Kikuo Takahashi, and Mr. Norio Ito with the technical division of the institute.

*Present address: JFE Engineering Co., Tokyo 100-0005, Japan.

[1] R. D. Richtmyer, Commun. Pure Appl. Math. **13**, 297 (1960).
[2] E. E. Meshkov, Izv. Akad. Nauk. SSSR. Mekh. Zhidk. Gaza **4**, 151 (1969) [Soviet Fluid Dynamics **4**, 101 (1969)].
[3] V. Rupert, in *Proceedings of the 18th International Symposium on Shock Waves*, edited by K. Takayama (Springer-Verlag, Heidelberg, Germany, 1992), p. 83.
[4] R. L. Holmes *et al.*, J. Fluid Mech. **389**, 55 (1999).
[5] M. Brouillette and B. Sturtevant, Physica (Amsterdam) **37D**, 248 (1989).
[6] S. Zaytsev, E. Chebotareva, and S. Titov, in *Proceedings of the 19th International Symposium on Shock Waves*, edited by R. Brun and L. Z. Dumitrescu (Springer, Heidelberg, 1995), p. 227.
[7] S. G. Zaitsev *et al.*, Sov. Phys. Dokl. **30**, 579 (1985).
[8] J. K. Prasad *et al.*, Phys. Fluids **12**, 2108 (2000).
[9] J. D. A. Holder, A. V. Smith, C. J. Barton, and D. L. Youngs, Laser Part. Beams **21**, 411 (2003).
[10] D. A. Holder *et al.*, Laser Part. Beams **21**, 403 (2003).
[11] V. A. Andronov *et al.*, Sov. Phys. JETP **44**, 424 (1977).
[12] O. Sadot *et al.*, Phys. Rev. Lett. **80**, 1654 (1998).
[13] L. Erez *et al.*, Shock Waves **10**, 241 (2000).
[14] S. H. R. Hosseini and K. Takayama, Phys. Fluids **17**, 084101 (2005).
[15] G. Layes, G. Jourdan, and L. Houas, Phys. Rev. Lett. **91**, 174502 (2003).
[16] Y. A. Kucherenko *et al.*, Laser Part. Beams **21**, 389 (2003).
[17] J. W. Jacobs, Phys. Fluids A **5**, 2239 (1993).
[18] K. Prestridge *et al.*, Exp. Fluids **29**, 339 (2000).
[19] S. Kumar *et al.*, Phys. Fluids **17**, 082107 (2005).
[20] M. A. Jones and J. W. Jacobs, Phys. Fluids **9**, 3078 (1997).
[21] J. W. Jacobs and V. V. Krivets, Phys. Fluids **17**, 034105 (2005).
[22] M. Brouillette and R. Bonazza, Phys. Fluids **11**, 1127 (1999).
[23] G. Jourdan and L. Houas, Phys. Fluids **8**, 1353 (1996).
[24] L. Houas and I. Chemouni, Phys. Fluids **8**, 614 (1996).
[25] G. N. Sankin, W. N. Simmons, S. L. Zhu, and P. Zhong, Phys. Rev. Lett. **95**, 034501 (2005).
[26] X. Yu, T. Ohtani, S. Kim, T. Ogawa, I.-S. Jeung, and A. Sasoh, Sci. Tech. Energetic Mater. **66**, 274 (2005).
[27] See EPAPS Document No. E-PRLTAO-97-066646 for video file of Fig. 2; the right-bottom number equals t in μs. For more information on EPAPS, see http://www.aip.org/pubservs/epaps.html.
[28] J. F. Kielkopf, Phys. Rev. E **63**, 016411 (2000).
[29] N. G. Glumac, G. S. Elliott, and M. Boguszko, AIAA J. **43**, 1984 (2005).
[30] I. G. Dors and C. G. Parigger, Appl. Opt. **42**, 5978 (2003).
[31] V. Svetsov *et al.*, Shock Waves **7**, 325 (1997).
[32] D. Nassif and L. Huwel, J. Appl. Phys. **87**, 2127 (2000).
[33] K. Mori, K. Komurasaki, and Y. Arakawa, J. Appl. Phys. **95**, 5979 (2004).
[34] K. Mori, T. Ohtani, and A. Sasoh, Trans. Jpn. Soc. Mech. Engineers (to be published).
[35] H. Bonde, Phys. Fluids **2**, 217 (1959).
[36] E. T. Pitkin, Acta Astronaut. **4**, 1137 (1977).
[37] G. Taylor, Proc. R. Soc. A **201**, 192 (1950).
[38] S. Chandrasekhar, *Hydrodynamic and Hydromagnetic Stability* (Dover Publications Inc., New York, 1961), Chap. 10.